Mineralogical Magazine (2023), **87**, 194–203
doi:10.1180/mgm.2022.140

CAMBRIDGE UNIVERSITY PRESS

Article

Thermodynamics and crystal structures of krautite, $Mn[AsO_3(OH)]\cdot H_2O$, koritnigite, $Zn[AsO_3(OH)]\cdot H_2O$ and cobaltkoritnigite, $Co[AsO_3(OH)]\cdot H_2O$

Juraj Majzlan[1], Jakub Plášil[2] and Edgar Dachs[3]

[1]Institute of Geosciences, Friedrich-Schiller University, Burgweg 11, 07749 Jena, Germany; [2]Institute of Physics of the CAS, v.v.i., Na Slovance 1999/2, 18220 Prague 8, Czech Republic; and [3]Department of Chemistry and Physics of Materials, University of Salzburg, Jakob-Haringer-Strasse 2a, 5020 Salzburg, Austria

Abstract

Synthetic samples of krautite, $Mn[AsO_3(OH)]\cdot H_2O$, koritnigite, $Zn[AsO_3(OH)]\cdot H_2O$ and cobaltkoritnigite, $Co[AsO_3(OH)]\cdot H_2O$, were used for calorimetric experiments. For krautite and koritnigite, single-crystal X-ray diffraction was used to determine positions of all atoms, including the H atoms. These data allowed the hydrogen-bond network and the function of H_2O molecules in these structures to be determined. The structural formulae are $Mn_4(H_2{}^{[3]}O)_4[AsO_3(OH)]_4$ and $Zn_4(H_2{}^{[3]}O)_2[AsO_3(OH)]_4(H_2{}^{[4]}O)_2$, where $^{[3]}H_2O$ and $^{[4]}H_2O$ are the 'transformer' and 'non-transformer' H_2O groups, respectively. Even though the principal features of these structures are identical, the details, especially those regarding the H_2O groups, differ from one structure to another structure in this group. The solubility products (log K_{sp}) were determined from calorimetric data, that is, from the experimentally measured enthalpies of formation and entropies. They relate to the reaction $M[AsO_3(OH)]\cdot H_2O \rightarrow M^{2+} + HAsO_4^{2-} + H_2O$ and are –6.10 for krautite, –6.88 for koritnigite and –6.83 for cobaltkoritnigite. We also estimated the log K_{sp} for magnesiokoritnigite as –2.0. Calculation of phase diagrams shows that all these phases originate under acidic conditions from solutions with high metal and arsenate concentration. They are restricted to local environments, to pockets that maintain such high concentrations over the time necessary for crystallisation of the krautite-group phases.

Keywords: krautite, koritnigite, thermodynamics, crystal structures, hydrogen bonding

(Received 1 June 2022; accepted 10 December 2022; Accepted Manuscript published online: 21 December 2022; Associate Editor: Sergey V Krivovichev)

Introduction

Natural arsenates constitute a large, chemically and structurally variable group of minerals (Drahota and Filippi, 2009; Majzlan *et al.*, 2014). They can accommodate many divalent metals in various structural types. The vivianite-group arsenates, for example, have the general formula $M_3(AsO_4)_2\cdot 8H_2O$, where M = Ni, Co, Zn, Mg, Mn, Fe and Cu (Sejkora *et al.*, 2014; Plášil *et al.*, 2017; Ciesielczuk *et al.*, 2018; Siuda and Macioch, 2018; Dumańska-Słowik *et al.*, 2018). Natural members of this group are mostly Ni or Co rich. The olivenite group with the general formula $M_2(AsO_4)OH$ includes members with M = Cu, Zn or Mn, although only the Cu- and Zn-rich compositions are more common in Nature (Southwood *et al.*, 2020). Minerals of the roselite and fairfieldite group with the general formula $Ca_2M(AsO_4)_2\cdot 2H_2O$ are less common and include members with M = Co, Mn, Zn, Cu, Ni and Mg (Fleck *et al.*, 2002). The krautite group, the subject of this work, hosts $M(AsO_3OH)\cdot H_2O$ minerals with M = Mn, Zn, Co, Mg and Ca. The group is not structurally homogeneous. The structures contain heteropolyhedral sheets with similar, but not identical topology. The sheets must accommodate the coordination requirements of the different divalent cations.

The selection of the phases and their metals is controlled by a combination of geochemical parameters (composition of the primary minerals), physico-chemical properties of the aqueous fluids (e.g. pH) and thermodynamics of the solids. The relative importance of such variables can be judged by detailed investigations of mineral-rich, classical localities, such as Jáchymov in the Czech Republic (Škácha *et al.*, 2019), associated solutions (e.g. Majzlan *et al.*, 2020) and thermodynamic measurements. Zinc and cobalt for such minerals are released by weathering of primary ore minerals. Manganese, on the other hand, could be released from minerals of ore deposits (Holtstam *et al.*, 2022; Cámara *et al.*, 2023) but could have other sources in the environment (e.g. Gatuingt *et al.*, 2021).

This work focuses on thermodynamic properties and crystal structures on selected synthetic equivalents of the minerals in the krautite group. Enthalpies of formation and entropies were measured by acid-solution and relaxation calorimetry, respectively. The data set was augmented by previously acquired data for some of the krautite-group phases (Plumhoff *et al.*, 2020; Majzlan *et al.*, 2020) and estimates for some phases. Phase

***Author for correspondence:** Juraj Majzlan, Email: Juraj.Majzlan@uni-jena.de
Cite this article: Majzlan J., Plášil J. and Dachs E. (2023) Thermodynamics and crystal structures of krautite, $Mn[AsO_3(OH)]\cdot H_2O$, koritnigite, $Zn[AsO_3(OH)]\cdot H_2O$ and cobaltkoritnigite, $Co[AsO_3(OH)]\cdot H_2O$. *Mineralogical Magazine* **87**, 194–203. https://doi.org/10.1180/mgm.2022.140

diagrams document the stability fields of these minerals and their formation conditions. Single-crystal X-ray diffraction experiments were used to determine the position of all atoms (including the H atoms) in these structures and to understand hydrogen bonding schemes in these phases.

Materials

Synthetic krautite was prepared by a method outlined in Buckley *et al.* (1990), specified already by Catti and Franchini-Angela (1979) and Deiss (1914). One solution was prepared by mixing and dissolving 4.5 g KH_2AsO_4 in 20 mL water. Another solution was prepared with 4.95 g $MnCl_2{\cdot}4H_2O$ and 20 mL water. The arsenical solution was heated slightly to dissolve the solid completely. The two solutions were mixed rapidly and turned immediately to a thick gel. Aggregates of pink krautite crystals grew in the gel. After two months, parts of the gel started to turn to liquid and released some of the aggregates (Fig. 1a). They were picked up with tweezers, dried with a paper towel and examined under binocular microscope for morphology or colour that deviate from that of krautite.

Koritnigite was synthesised by the same procedure, taking 3.41 g $ZnCl_2$ instead of the manganese chloride. Again, thick gel formed and turned slowly to liquid. In this case, even after one year, more than half of the volume still consisted of gel, however a sufficient number of crystals (Fig. 1b) were available for all analyses.

A similar synthesis was attempted with $CoCl_2{\cdot}6H_2O$ but the gel remained thick and essentially unchanged for more than one year. No crystals were seen in the purple, compact gel. Therefore, cobaltkoritnigite was prepared by the procedure described by Zettler *et al.* (1979). As specified therein, 0.33 g As_2O_5 and 1.4 g $CoSO_4{\cdot}7H_2O$ were mixed with 5 mL water and maintained in a Teflon-lined pressure bomb at 150°C for six days. Afterwards, the bomb was allowed to cool slowly to room temperature and the crystals (Fig. 1c) were filtered from the remaining liquid.

Methods

Selected single crystals were investigated by a Rigaku SuperNova single-crystal diffractometer equipped with the Atlas S2 detector and using the mirror-monochromatised Mo$K\alpha$ radiation ($\lambda = 0.71073$ Å) from a micro-focus X-ray tube. Correction for background, Lorentz effect and polarisation, as well as the empirical (multi-scan) absorption correction were applied to the data during reduction in the *CrysAlis* package (Rigaku v.2018). The structure has been solved independently from previous structure investigations (Catti and Franchini-Angela, 1979; Keller *et al.*, 1980) using an intrinsic-phasing algorithm of the program *SHELXT* (Sheldrick, 2015) and subsequently treated by the least-squares refinement in *Jana2020* (Petříček *et al.*, 2020).

The aggregates of crystals used for calorimetry were ground to powder and tested for their purity with a Bruker D8 ADVANCE powder X-ray diffractometer with DAVINCI design, and with Cu$K\alpha$ radiation, Ni filter and a Lynxeye 1D detector. A step size of 0.02°2θ and a 0.25 s per step were used. Lattice parameters were refined using *JANA2006* (Petříček *et al.*, 2014).

Acid-solution calorimetry and relaxation calorimetry were used to measure enthalpies of dissolution in 5 N HCl and low-temperature heat capacities, respectively. Both methods were used in an identical fashion as in our previous work (e.g. Majzlan *et al.*, 2020). The details on acid-solution calorimetry of secondary minerals are summarised by Majzlan (2017). The principles of relaxation calorimetry, the accuracy and precision of the method have been described and evaluated by Dachs and Benisek (2011) and Kennedy *et al.* (2007).

Results

Crystal structure of koritnigite

A prismatic large, $0.140 \times 0.099 \times 0.023$ mm, fragment of synthetic koritnigite crystal (also used for calorimetric study) was investigated. The structure solution revealed nearly all atomic positions except those of the H atoms. Those were localised subsequently from the difference-Fourier maps and refined keeping soft constraints of 1.00 Å on the O–H distances as well as H–O–H angles, 105° within the H_2O molecules, and with the U_{iso} of each H set to 1.2 times that of the donor O atom. The final refinement including 265 parameters, 12 restraints and 12 constraints, converged to $R = 0.0270$ and $wR = 0.0663$ for 3330 unique observed reflections, of $I > 3\sigma(I)$, with goodness of fit = 1.37. The structure was modelled as twinned due to reticular merohedry (see Petříček *et al.*, 2016) as a two-component twin (Table 1). Crystallographic details, data collection and refinement parameters are given in Table 1. The bond-valence analysis (after Brown 2002) is provided in Supplementary Table S1, based on the refined interatomic distances (Supplementary Table S2) and the

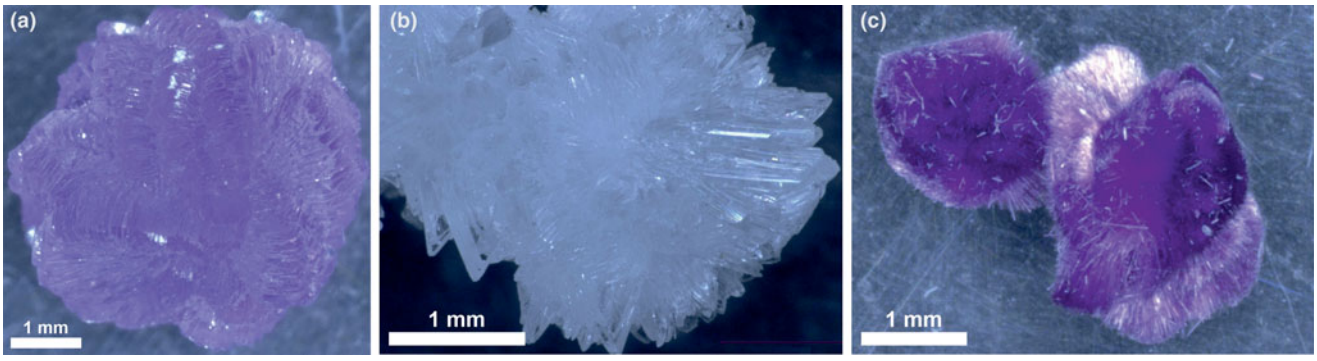

Fig. 1. Aggregates of synthetic (a) krautite, (b) koritnigite and (c) cobaltkoritnigite.

https://doi.org/10.1180/mgm.2022.140 Published online by Cambridge University Press

Table 1. Crystal data, collection and refinement parameters for synthetic koritnigite and krautite.

	Koritnigite	Krautite
Crystal data		
Chemical formula	$Zn_4(H_2^{[3]}O)_2[(AsO_3(OH)]_4(H_2^{[4]}O)_2$	$Mn_4(H_2^{[3]}O)_3[(AsO_3(OH)]_4(H_2^{[4]}O)$
M_r	893.28	851.52
Crystal system, space group	triclinic, $P\bar{1}$	monoclinic, $P2_1$
Temperature (K)	298	297
a, b, c [Å]	7.9249(6), 15.7809(3), 6.6407(3)	8.0034(3), 15.9559(11), 6.8068(6)
α, β, γ [°]	89.688(3), 96.5460(3), 90.007(3)	90, 96.424(8), 90
V [Å^3]	825.07(7)	863.78(13)
Z	2	2
Radiation type	Mo$K\alpha$ radiation, λ = 0.71073 Å	Mo$K\alpha$ radiation, λ = 0.71073 Å
μ (mm^{-1})	13.81	10.56
Crystal size [mm]	0.140 × 0.099 × 0.023	0.093 × 0.054 × 0.007
Data collection		
Diffractometer	Rigaku SuperNova with Atlas S2 detector	Rigaku SuperNova with Atlas S2 detector
Absorption correction	multi-scan	multi-scan
T_{min}, T_{max}	0.506, 1	0.715, 1
No. of measured, independent and observed [$I > 3\sigma(I)$] reflections	22576, 3690, 3300	12476, 4564, 3895
Range of hkl	$h = -10\rightarrow10$, $k = -20\rightarrow20$, $l = -8 \rightarrow 8$	$h = -11\rightarrow11$, $k = -21\rightarrow21$, $l = -9 \rightarrow 9$
R_{int}	0.043	0.038
(Sin θ/λ)$_{max}$(Å^{-1})	0.6529	0.6971
Refinement		
$R[F^2 > 3\sigma(F^2)]$, $wR(F^2)$, S	0.0270, 0.0663, 1.37	0.0338, 0.0666, 1.24
Weighting scheme, weights	σ, $w = 1/(\sigma^2(I)+0.029307P^2)$, where $P = (F_o^2+2F_c^2)/3$	σ, $w = 1/(\sigma^2(I)+0.020978P^2)$, where $P = (F_o^2+2F_c^2)/3$
No. of reflections	3690	4564
No. of parameters	265	284
No. of restraints	12	15
H-atom treatment	All H-atoms parameters refined	All H-atoms parameters refined
$\Delta\rho_{max}$, $\Delta\rho_{min}$ (e^- Å^{-3})	0.42, −0.45	0.59, −0.38
Twin matrices; fractions	$\begin{pmatrix}\bar{1}&0&0\\0&1&0\\0&0&\bar{1}\end{pmatrix}$; 0.503(3) / 0.497(3)	$\begin{pmatrix}\bar{1}&0&0\\0&\bar{1}&0\\0&0&\bar{1}\end{pmatrix}$; 0.6474(17) / 0.326(17)
Absolute structure; Flack parameter	–	2156 Friedel pairs; 0.33(2)

bond-valence parameters given by Gagné and Hawthorne (2015). Hydrogen-bond geometry is summarised in Supplementary Table S3. The crystallographic information file has been deposited with the Principal Editor of *Mineralogical Magazine* and is available as Supplementary material (see below).

Crystal structure of krautite

A short-prismatic, 0.093 × 0.054 × 0.007 mm, fragment of synthetic krautite crystal (also used for calorimetric study) was investigated. The structure solution revealed nearly all atomic positions except those of the H atoms. The structure is non-centrosymmetric, of the space-group $P2_1$; the absolute structure has been refined (as an inversion-twin). Afterwards, the positions of all H atoms have been successfully localised from the difference-Fourier maps corrected for the F^2 from the second twin-domain contribution (Petříček *et al.*, 2016). H atoms were refined keeping soft constraints of 1.00 Å on the O–H distances as well as H–O–H angles, 105° within the H_2O molecules, and with the U_{iso} of each H set to 1.2 times that of the donor O atom. The final refinement including 284 parameters, 15 restraints and 19 constraints, converged to $R = 0.0338$ and $wR = 0.0666$ for 3895 unique observed reflections, of $I > 3\sigma(I)$, with goodness of fit = 1.24. Crystallographic details, data collection and refinement parameters are given in Table 1. The bond-valence analysis (after Brown, 2002) is provided in Supplementary Table S4, based on the refined interatomic distances (Supplementary Table S5) and the bond-valence parameters given by Gagné and Hawthorne (2015). The hydrogen-bond geometry is summarised in Supplementary Table S6. The crystallographic information file and the structure factors list have been deposited with the Principal Editor of Mineralogical Magazine and are available as Supplementary material (see below).

Thermodynamic measurements

Apart from the title compounds, additional phases must be measured in order to convert the dissolution enthalpies to enthalpies of formation. These additional phases, so-called reference phases, were ZnO, MnO, $CoSO_4{\cdot}7H_2O$, KH_2AsO_4, $HCl{\cdot}9.96H_2O$, H_2O and KCl. The enthalpies of dissolution of all these phases in 5 N HCl are given in Table 2, together with an appropriate thermochemical cycle. The calculated enthalpies of formation are listed in Table 3.

The low-temperature heat capacities (Fig. 2a) were measured and integrated for koritnigite (Supplementary Tables S7, S8) and krautite (Supplementary Tables S9, S10). Thermodynamic functions calculated from the smoothed C_p data are presented in Supplementary Tables S8 and S10. Both data sets show anomalies at very low temperatures. In the data for koritnigite, there is a very weak, broad C_p anomaly at 3 K. The nature of this anomaly is unclear but its contribution to overall C_p and S is negligible.

In the data for krautite, there is a sharp lambda-shaped anomaly at 3 K (Fig. 2b). This anomaly can be assigned to the magnetic ordering below this temperature. The position of the anomaly is

https://doi.org/10.1180/mgm.2022.140 Published online by Cambridge University Press

Table 2. Thermochemical cycle and the enthalpies of the individual reactions used in this work. The bottom portion of the table lists the equations needed for the calculation of formation enthalpies of the arsenates of the krautite group.

Reaction	Reaction number
$M[AsO_3(OH)]\cdot H_2O$ (cr) → M^{2+} (aq) + H^+ (aq) + AsO_4^{3-} (aq) + H_2O (aq)	1
MO (cr) + $2H^+$ (aq) → M^{2+} (aq) + H_2O (aq)	2
$CoSO_4\cdot 7H_2O$ (cr) → Co^{2+} (aq) + SO_4^{2-} (aq) + $7H_2O$ (aq)	3
$MgSO_4$ (cr) → Mg^{2+} (aq) + SO_4^{2-} (aq)	4
KH_2AsO_4 (cr) → K^+ (aq) + $2H^+$ (aq) + AsO_4^{3-} (aq)	5
$HCl\cdot 9.96H_2O$ (l) → H^+ (aq) + Cl^- (aq) + $9.96H_2O$ (aq)	6
H_2O (l) → H_2O (aq)	7
KCl (cr) → K^+ (aq) + Cl^- (aq)	8
M (cr) + (½)O_2 (g) → MO (cr)	9
$CoSO_4\cdot 7H_2O$ (cr) → Co^{2+} (aq) + SO_4^{2-} (aq) + $7H_2O$ (aq)	10
$MgSO_4$ (cr) → Mg^{2+} (aq) + SO_4^{2-} (aq)	11
K (cr) + As (cr) + H_2 (g) + $2O_2$ (g) → KH_2AsO_4 (cr)	12
$10.46H_2$ (g) + $9.96O_2$ (g) + (½)Cl_2 (g) → $HCl\cdot 9.96H_2O$ (l)	13
H_2 (g) + (½)O_2 (g) → H_2O (l)	14
K (cr) + (½)Cl_2 (g) → KCl (cr)	15
M (cr) + As (cr) + $2.5O_2$ (g) + $1.5H_2$ (g) → $M[AsO_3(OH)]\cdot H_2O$ (cr)	16
Dissolution/dilution enthalpies	**Formation enthalpies**
$\Delta H_{1,Mn} = \Delta_{diss}H$(krautite) = 0.09±0.11(2)	
$\Delta H_{1,Zn} = \Delta_{diss}H$(koritnigite) = 10.20±0.05(6)	
$\Delta H_{1,Co} = \Delta_{diss}H$(cobaltkoritnigite) = −8.55±0.07(2)	
$\Delta H_{2,Mn} = \Delta_{diss}H(MnO)$ = −113.35±0.05(3)	$\Delta H_{9,Mn} = \Delta_fH°(MnO,cr)$ = −385.2±0.5
$\Delta H_{2,Zn} = \Delta_{diss}H(ZnO)$ = −70.24±0.11(3)	$\Delta H_{9,Zn} = \Delta_fH°(ZnO,cr)$ = −350.5±0.3
$\Delta H_{2,Mg} = \Delta_{diss}H(MgO)$ = −149.68±0.60(9)	$\Delta H_{9,Mg} = \Delta_fH°(MgO,cr)$ = −601.6±0.3
$\Delta H_3 = \Delta_{diss}H(CoSO_4\cdot 7H_2O)$ = 44.66±0.31(6)	$\Delta H_{10} = \Delta_fH°(CoSO_4\cdot 7H_2O,cr)$ = −2979.3±1.5
$\Delta H_4 = \Delta_{diss}H(MgSO_4)$ = −53.50±0.48(7)	$\Delta H_{11} = \Delta_fH°(MgSO_4,cr)$ = −1288.64±1.28
$\Delta H_5 = \Delta_{diss}H(KH_2AsO_4)$ = 24.75±0.18(10)	$\Delta H_{12} = \Delta_fH°(KH_2AsO_4,cr)$ = −1181.2±2.0
ΔH_6 = 0	$\Delta H_{13} = \Delta_fH°(HCl\cdot 9.96H_2O,l)$ = −3007.9±1.0
ΔH_7 = −0.54	$\Delta H_{14} = \Delta_fH°(H_2O,l)$ = −285.8±0.1
ΔH_8 = 17.69±0.06(31)	$\Delta H_{15} = \Delta_fH°(KCl,cr)$ = −436.5±0.2
Calculation of formation enthalpies	
$\Delta_fH°$(cobaltkoritnigite) = $-\Delta H_{1,Co} + \Delta H_3 + \Delta H_5 + \Delta H_{2,Mg} + \Delta H_6 - \Delta H_4 - \Delta H_8 - 16.96\Delta H_7 + \Delta H_{10} + \Delta H_{12} + \Delta H_{9,Mg} + \Delta H_{13} - \Delta H_{11} - \Delta H_{15} - 16.96\Delta H_{14}$	
$\Delta_fH°$(koritnigite) = $-\Delta H_{1,Zn} + \Delta H_{2,Zn} + \Delta H_5 + \Delta H_6 - \Delta H_8 - 9.96\Delta H_7 + \Delta H_{9,Zn} + \Delta H_{12} + \Delta H_{13} - \Delta H_{15} - 9.96\Delta H_{14}$	
$\Delta_fH°$(krautite) = $-\Delta H_{1,Mn} + \Delta H_{2,Mn} + \Delta H_5 + \Delta H_6 - \Delta H_8 - 9.96\Delta H_7 + \Delta H_{9,Mn} + \Delta H_{12} + \Delta H_{13} - \Delta H_{15} - 9.96\Delta H_{14}$	

Table 3. Summary of the thermodynamic data for the minerals of the krautite group.

	log K[a]	$\Delta_fH°$ kJ·mol^{-1}	S° J·mol^{-1}·K^{-1}	$\Delta_fS°$ J·mol^{-1}·K^{-1}	$\Delta_fG°$ kJ·mol^{-1}
Geminite	−6.99[b]				
$Cu[AsO_3(OH)]\cdot H_2O$					
Krautite	−6.10	−1392.2	178.1	−598.5	−1213.8
$Mn[AsO_3(OH)]\cdot H_2O$		±2.5	±1.2	±1.5	±2.6
	−6.7 to −6.9[c]				
Koritnigite	−6.88	−1324.5	158.6	−627.6	−1137.4
$Zn[AsO_3(OH)]\cdot H_2O$		±2.5	±1.1	±1.4	±2.5
Cobaltkoritnigite	−6.83	−1224.6	169.7	−604.9	−1044.3
$Co[AsO_3(OH)]\cdot H_2O$		±3.6	±3.0	±3.1	±3.7
Haidingerite	−3.21[d]				
$Ca[AsO_3(OH)]\cdot H_2O$					
Magnesiokoritnigite	−2.0[e]				
$Mg[AsO_3(OH)]\cdot H_2O$					
Fluckite	no data available				
$Ca_{0.5}Mn_{0.5}[AsO_3(OH)]\cdot H_2O$					

[a]All log K_{sp} values refer to a dissolution reaction $M[AsO_3(OH)]\cdot H_2O \rightarrow M^{2+} + HAsO_4^{2-} + H_2O$
[b]Plumhoff *et al.* (2020)
[c]calculated from Tournassat *et al.* (2002)
[d]Majzlan *et al.* (2020)
[e]estimated, see text

in excellent agreement with magnetic-susceptibility data of Bramwel *et al.* (1988). They determined that synthetic krautite is antiferromagnetic, with a Curie temperature of 3.2 K.

The presence of the anomalies complicated the fitting necessary to extract entropies for the two phases. There are no appropriate functions for the fitting of the lambda-shaped anomalies (e.g. Shapiro *et al.*, 1999). Both data sets were fitted with a series of polynomials that have no physical meaning. The polynomials were joined at temperatures where the differences in smoothed C_p and their slopes were minimal. These polynomial

https://doi.org/10.1180/mgm.2022.140 Published online by Cambridge University Press

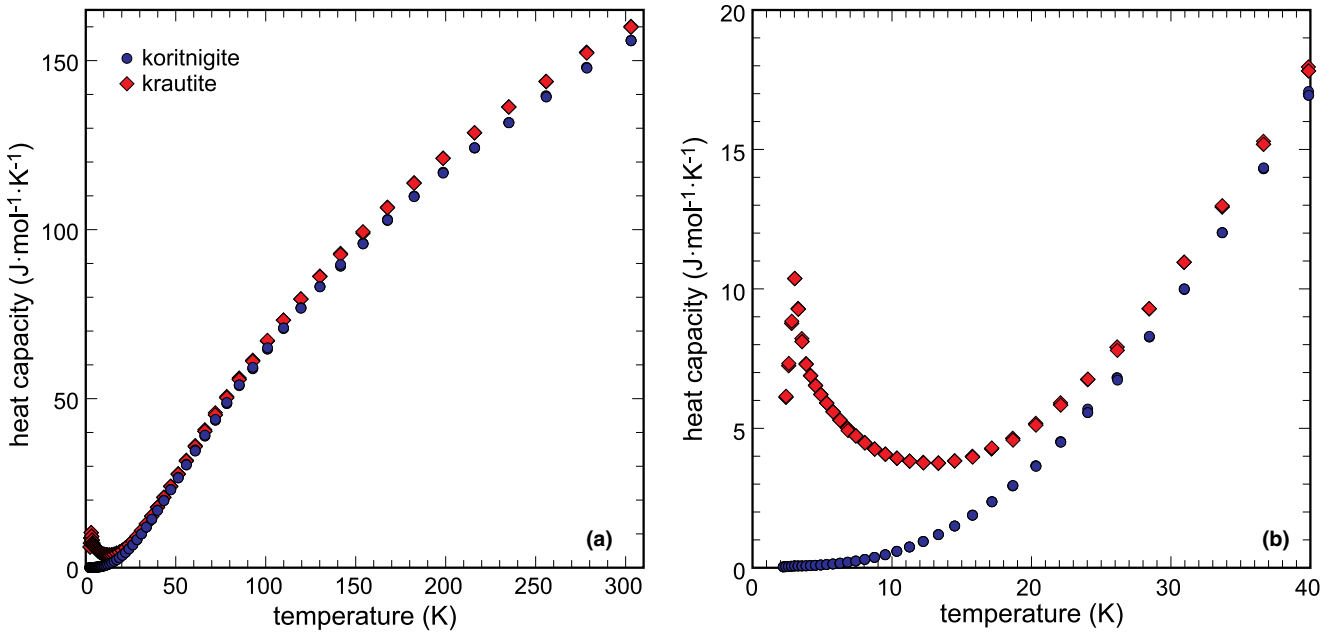

Fig. 2. Experimentally measured heat capacity of koritnigite and krautite. The panel (a) shows the full data sets and (b) shows a detail at low temperatures.

segments were then used to calculate thermodynamic functions between 0 and 300 K and the results are listed in Tables S8 and S10.

The calculated entropies were converted to entropies of formation, using the entropies of pure elements in their standard state from Robie and Hemingway (1995). Enthalpies and entropies of formation were then used to calculate the Gibbs free energies of formation (Table 3) and the solubility products, using auxiliary data from Robie and Hemingway (1995) and Nordstrom *et al.* (2014).

Entropy estimate for cobaltkoritnigite

In the absence of low-temperature heat capacity data for $Co[AsO_3(OH)]\cdot H_2O$, its entropy can be estimated from solid-state reactions:

$$M'[AsO_3(OH)]\cdot H_2O + M''O = M''[AsO_3(OH)]\cdot H_2O + M'O,$$

where M' and M'' are two different divalent metals. We have chosen oxides MO because of their simple structures and accurately known entropies. Because all phases that participate in this reaction are solids, it could be assumed that the entropy change associated with this reaction (Δ_rS) is 0 $J\cdot mol^{-1}\cdot K^{-1}$. This assumption can be tested for M' = Zn and M'' = Mn with the data from this work and entropies for simple oxides from Robie and Hemingway (1995). The calculated $\Delta_rS_{Zn-Mn} = 3.0\pm1.7$ $J\cdot mol^{-1}\cdot K^{-1}$, a small entropy value. The reason for the small difference could be a different structural type for MnO (halite) and ZnO (wurtzite). For the estimate for cobaltkoritnigite, pairs of MnO–CoO (both halite structures) and ZnO–CoO (different structure types) can be tested. Assuming that Δ_rS_{Zn-Co} and Δ_rS_{Mn-Co} are both 0 $J\cdot mol^{-1}\cdot K^{-1}$, the entropy of $Co[AsO_3(OH)]\cdot H_2O$ can be estimated as 168.2 and 171.2 $J\cdot mol^{-1}\cdot K^{-1}$, respectively. Hence, even though there is a structural difference between ZnO and CoO, the entropy estimate is similar to that obtained from the calculation with the MnO–CoO pair. We adopted the average value 169.7 $J\cdot mol^{-1}\cdot K^{-1}$, with a conservative error estimate of ±3.0 $J\cdot mol^{-1}\cdot K^{-1}$.

Discussion

Role of H_2O in the crystal structures of solids

To analyse and evaluate the role of molecular water in the structures of solids, a useful scheme was introduced in the literature by Frank Hawthorne and co-workers (Hawthorne, 1992, 2012; Hawthorne and Schindler, 2008; Hawthorne and Sokolova, 2012; Schindler and Hawthorne, 2008). Generally, there are several types of H_2O moieties in crystal structures and each of them play a distinct role in structure bonding. Particular types of H_2O can be distinguished based on the coordination number of O atoms in these H_2O groups. In the structures of oxysalts, in general, there are 'transformer', 'non-transformer' and 'inverse' transformer H_2O groups with [3], [4] and [5]-fold coordinated O atoms, respectively. Their role is generally to transfer the bond-valence from cations (Lewis acids) to anions (Lewis bases), keeping the structure together, as the strengths of these components are equal or similarly matching, following the valence-matching principle of the bond-valence theory (Brown, 2002, 2009; Hawthorne 2012).

Symmetry of the structures of krautite and koritnigite

In this work, the crystal structure of krautite was refined in the monoclinic space group $P2_1$, in agreement with the earlier (Catti and Franchini-Angela, 1979) or newer (Weil *et al.*, 2022) models. On the other hand, other $M[AsO_3(OH)]\cdot H_2O$ structures with M = Co, Cu, Zn and Mg are triclinic (Keller *et al.*, 1980; Cooper and Hawthorne, 1995; Kampf *et al.*, 2013). The most recent addition to this group is a triclinic polymorph of $Mn[AsO_3(OH)]\cdot H_2O$ (Weil *et al.*, 2022), not known from Nature so far. The differences between the monoclinic and triclinic structures in this group of phases are subtle and seem to be related to the hydrogen-bonding scheme in these structures. Our refinements confirmed the choice of symmetry for krautite and koritnigite. There were no indications that the symmetry should be changed.

https://doi.org/10.1180/mgm.2022.140 Published online by Cambridge University Press

Crystal structure and hydrogen-bonding network of koritnigite

The structure of koritnigite has been determined first by Keller *et al.* (1980). It contains four Zn sites, four As sites, twenty O sites and twelve H sites. In the general view, the structure consists of zig-zag edge-sharing chains of $ZnO_5(H_2O)$ octahedra that run parallel to [10$\bar{1}$]. They are joined by corner-sharing with $AsO_3(OH)$ tetrahedra to form sheets parallel to {010} (Fig. 3). Two of the four vertices of each of the $AsO_3(OH)$ tetrahedra are O atoms of Zn-octahedra, while the other two are unlinked, except by hydrogen bonding. The sheets are linked in the [010] direction only by hydrogen bonds (Fig. 3). The Zn1 and Zn4 octahedra form one set of chains linked into a sheet centred at 0 along **b** and the Zn2 and Zn3 octahedra form another set of chains linked into a sheet centred at ½ along **b**.

The structure of koritnigite contains four symmetrically independent OH groups and four symmetrically independent H_2O molecules. Each of those H_2O molecules participates in the bonding within the single $ZnO_5(H_2O)$ octahedron. Those linked to Zn3 and Zn4 (O20 and O17 respectively; see Table S1) are transformer H_2O groups with the 3-coordinated O atom. On the other hand, the O15 and O11 that are linked to Zn1 and Zn2, respectively, seem to be non-transformer H_2O groups, as each of them accepts one additional weak H-bond from the interlayer. These findings are consistent with observations and predictions made by Keller *et al.* (1980) for koritnigite and by Kampf *et al.* (2013) for magnesiokoritnigite. Nevertheless, neither of these papers found H atoms from the diffraction data and were based only on the crystal-chemical considerations. The geometry of hydrogen bonds in the crystal structure of synthetic koritnigite is summarised in Supplementary Table S3. The structural formula of synthetic koritnigite is $Zn_4(H_2^{[3]}O)_2[AsO_3(OH)]_4(H_2^{[4]}O)_2$, Z = 2, $D_{calc.}$ = 3.5956 g cm^{-3}.

Crystal structure and hydrogen-bonding network of krautite

The structure of krautite has been first determined by Catti and Franchini-Angela (1979). It contains four Mn, four As and twenty O sites. Furthermore, it hosts twelve H atoms, associated with OH and H_2O, which have not been found in previous work. The structure consists of (010) layers composed of chains of $Mn\varphi_6$ octahedra running in the [101] direction (Fig. 4). These chains are interconnected by the As tetrahedra. Each of the four independent arsenate tetrahedra attaches to the octahedral chains *via* three oxygen atoms; the fourth oxygen is protonated, staggered towards the interlayer, and it participates in hydrogen-bonding between the layers (Fig. 4). Adjacent layers are held together only by hydrogen bonds resulting in the excellent (010) cleavage of krautite. The layers are stacked along and related by the screw 2_1 axis.

The structure of krautite contains four symmetrically independent OH groups and four symmetrically independent H_2O molecules in the asymmetric part of the unit cell. Similarly to koritnigite, each of those H_2O participates in the bonding within the single $MnO_5(H_2O)$ octahedron. Nevertheless, based on the current structure refinement it is likely that three H_2O groups within the krautite structure, O10 (Mn2), O13 (Mn3) and O20 (Mn4) (see Table S4), are transformer H_2O groups with a 3-coordinated O atom. The O7 atom seems to be a part of a non-transformer H_2O group with a fourfold coordinated O atom. The geometry of hydrogen bonds in the crystal structure of synthetic krautite is summarised in Table S6. The structural formula of synthetic krautite is $Mn_4(H_2^{[3]}O)_3[AsO_3(OH)]_4(H_2^{[4]}O)$, Z = 2, $D_{calc.}$ = 3.2739 g cm^{-3}.

The structural models of synthetic krautite from this work and that of Bramwell *et al.* (1994) are very similar. The calculated arithmetic mean (dav) of the equivalent atoms distances is 0.1331 Å. The measure of similarity (Δ) (after Bergerhoff *et al.*, 1999) is 0.012, which is a function of the differences in atomic positions, weighted by the multiplicities of the sites, and the ratios of the corresponding lattice parameters of the structures. The maximum difference in those two structures has been found for the atom H1O10 and is 0.6609 Å. This difference is seen as reasonable as we are comparing X-ray diffraction (this work) and neutron diffraction (Bramwell *et al.*, 1994) techniques.

Stability and formation conditions of koritnigite, krautite and related phases

The thermodynamic data acquired in this work allow for quantitative assessment of the stability of the $M[AsO_3(OH)]\cdot H_2O$, including krautite, koritnigite and cobaltkoritnigite, and comparison of these phases to the chemically related geminite $[Cu[AsO_3(OH)]\cdot H_2O]$ and haidingerite $[Ca[AsO_3(OH)]\cdot H_2O]$. Given the presence of the acidic $AsO_3(OH)$ group in their structures,

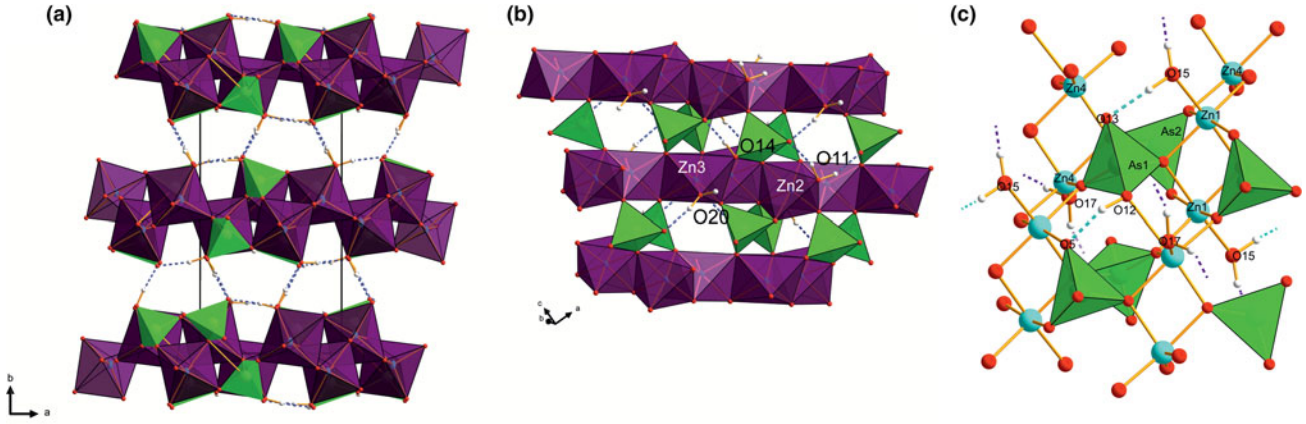

Fig. 3. Hydrogen-bonding in the structure of koritnigite. (a) $\{ZnO_5(H_2O)AsO_3(OH)\}^{\infty}$ sheets, stacked perpendicular to **b**, are linked *via* loose H-bonds only, whereas (b) the intrasheet H-bonding network is denser (shown is a single layer). Zn is in violet colour, As is green, blue dashed are H-bonds, H atoms are whitish. Unit-cell edges are outlined in black lines. (c) a detail of the intrasheet H-bonding network. Zn is in pale-green colour, As is green, pale-green dashed are H-bonds.

https://doi.org/10.1180/mgm.2022.140 Published online by Cambridge University Press

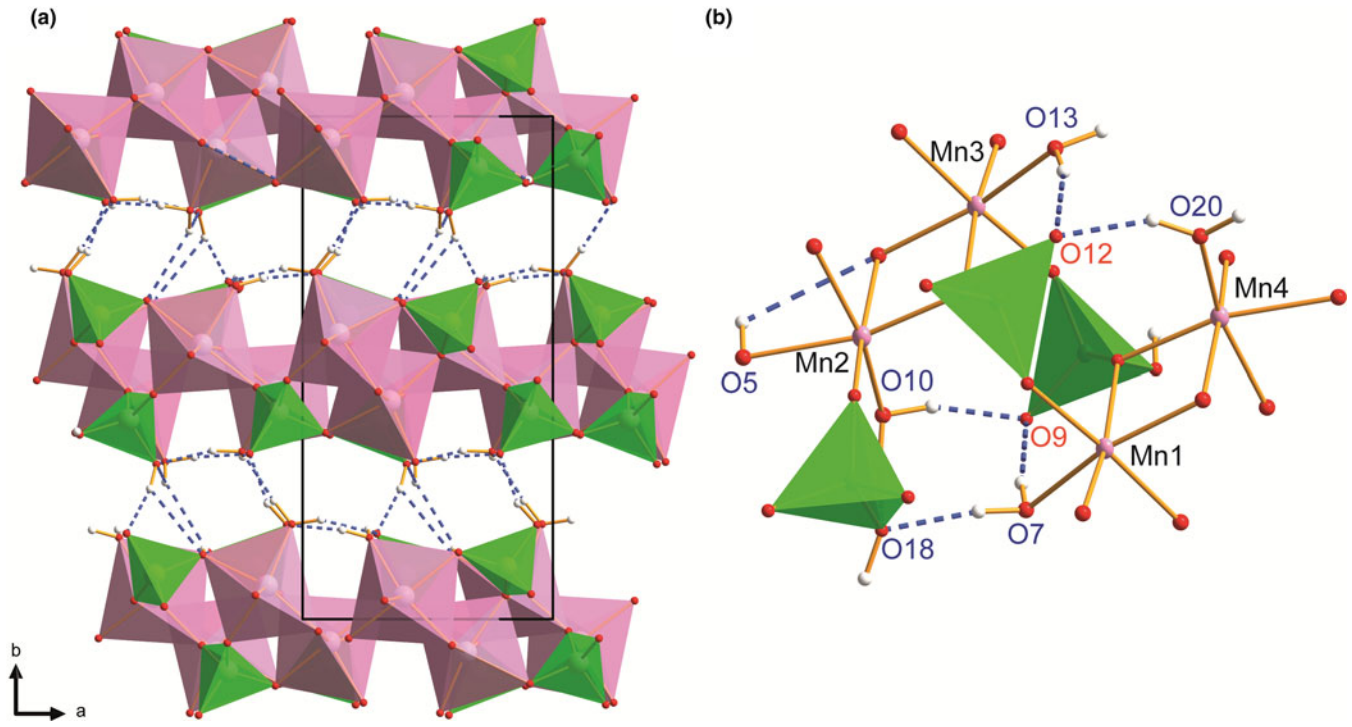

Fig. 4. Hydrogen-bonding in the structure of krautite. (a) $\{MnO_5(H_2O)AsO_3(OH)\}^{\infty}$ sheets, stacked perpendicular to **b**, are linked *via* loose H-bonds only, whereas (b) the intrasheet H-bonding network (detail only displayed) is dense and strong. Mn is light-pink colour, As is green, blue dashed are H bonds, labels in red belong to O^{2-} and blue to H_2O/OH. Unit-cell edges are outlined in black lines.

it is not surprising that they are predicted to crystallise from acidic solutions (Figs 5, 6). Another property, not obvious from their composition, is their relatively high solubility. Hence, in general, these phases precipitate from oxidised acidic (acid mine drainage) solutions with high metal and arsenic concentrations.

The best example is the system $ZnO–As_2O_5–H_2O$, with the phases koritnigite, köttigite [vivianite group, $Zn_3(AsO_4)_2{\cdot}8H_2O$] and adamite [olivenite group, $Zn_2(AsO_4)(OH)$]. Thermodynamic data for köttigite were taken from Lee and Nriagu (2007) and those for adamite from Magalhães *et al.* (1988). A phase diagram that represents only an oxidised solution (Fig. 5a, 6b) shows the relationships between the three zinc arsenates. The stability field of koritnigite is restricted to low pH values and high Zn and As concentrations. The greatest stability field belongs to

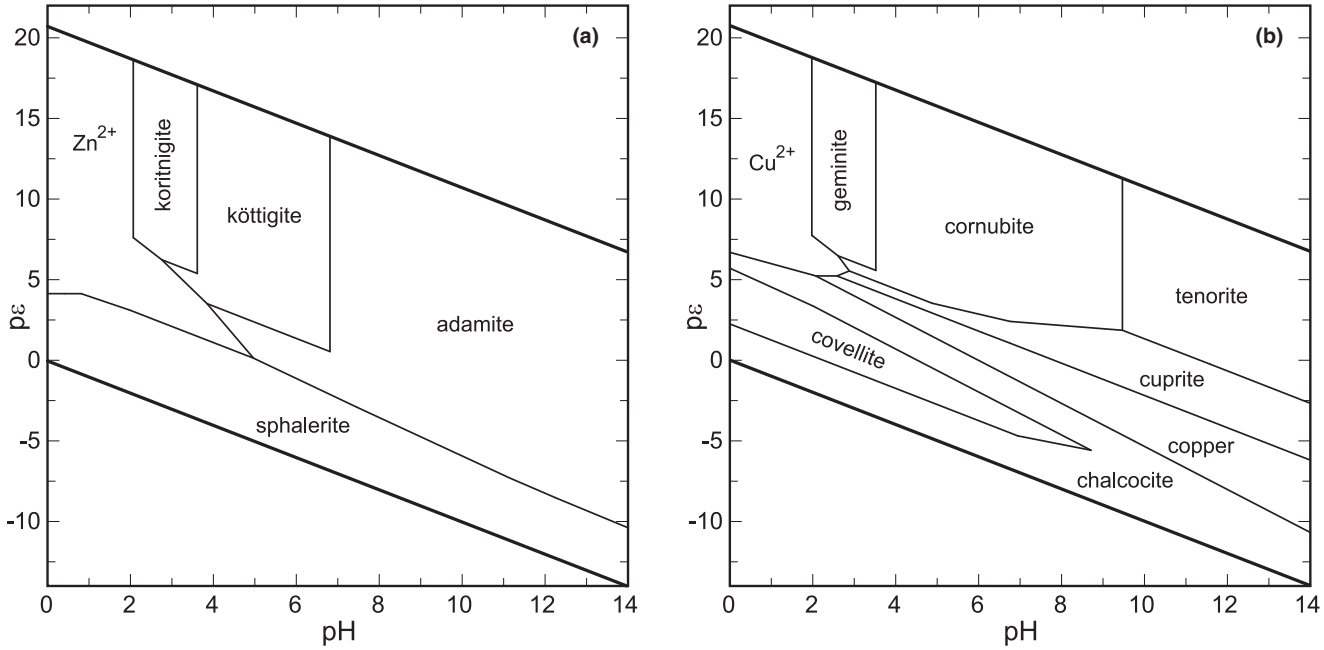

Fig. 5. pH–pε diagrams for the system (a) $ZnO–As_2O_5–H_2O–S$ and (b) $Cu–O_2–S–As_2O_5–H_2O$. Constructed for log a[Zn(II)] or log a[Cu(II)] = –1, log a[As(V)] = –1, log a(S) = –3 and T = 298.15 K.

https://doi.org/10.1180/mgm.2022.140 Published online by Cambridge University Press

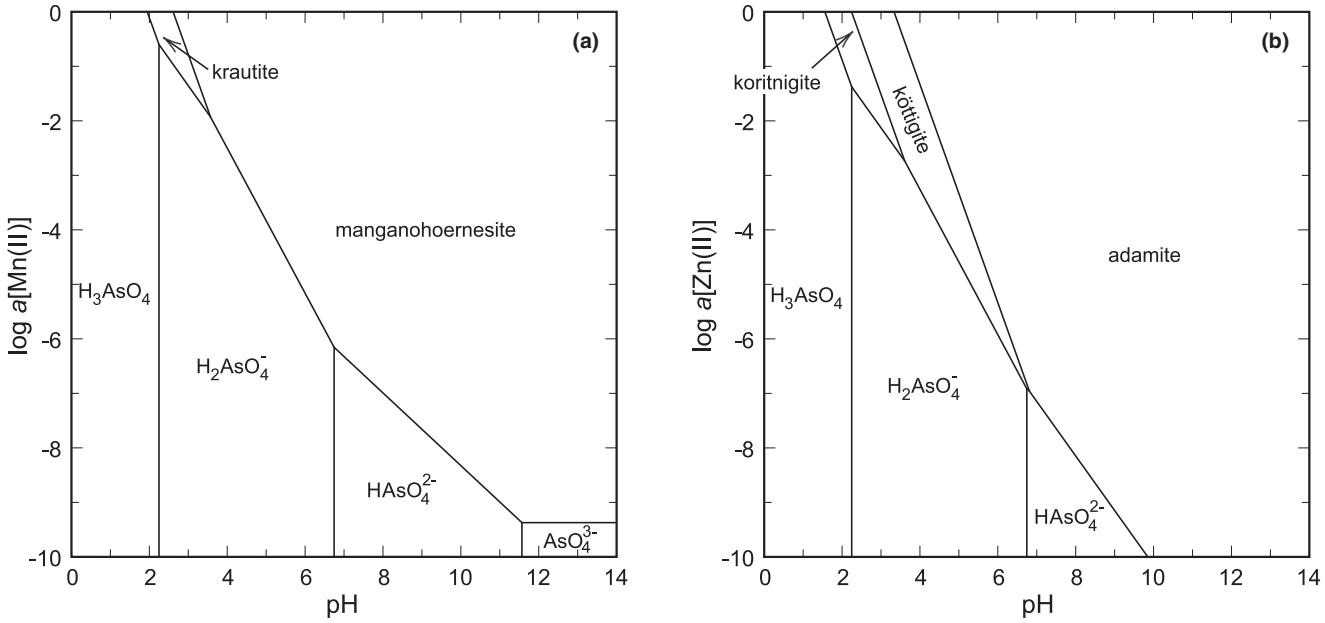

Fig. 6. pH-activity phase diagrams for the systems (a) MnO–As_2O_5–H_2O and (b) ZnO–As_2O_5–H_2O. Constructed for log a[As(V)] = –1 and T = 298.15 K.

adamite, a Zn arsenate that is much more common than koritnigite.

The evaluation in the system MnO–As_2O_5–H_2O is more difficult. The data for manganohörnesite [vivianite group, $Mn_3(AsO_4)_2{\cdot}8H_2O$] from Johnston and Singer (2007) are uncertain and there are no thermodynamic data for eveite [olivenite group, $Mn_2(AsO_4)(OH)$], to our best knowledge. There is another datum for the solubility product of krautite available (Tournassat *et al.*, 2002). Converting their data to the reaction used in this present work (see footnote in Table 3), their value of log K_{sp} is –6.7 to –6.9, comparing fairly well to our datum of –6.10. Calculations suggest that manganohörnesite is stable over most of the diagram (Fig. 6a). We have to emphasise that the thermodynamic data for eveite are not known and this phase, similarly to adamite in the system with zinc, could displace much of the stability field of manganohörnesite. A small field for krautite appears under low pH and high aqueous ion concentrations.

The system CuO–As_2O_5–H_2O is complex because of the number of phases, resulting from the flexibility of coordination of Cu^{2+} in their structures. The stable phase in the system is olivenite [$Cu_2(AsO_4)(OH)$], the mineral structurally very similar to adamite and eveite. The structural analogue of köttigite and manganohörnesite is the rare mineral babánekite [vivianite group, $Cu_3(AsO_4)_2{\cdot}8H_2O$] (Plášil *et al.*, 2017) for which no thermodynamic data are available. Lide (2005) gave a solubility product for $Cu_3(AsO_4)_2$, suggesting that it may perhaps relate to a phase such as babánekite, but implying that such a phase would be quite stable. Such stability is in stark contrast with the rare occurrence of such a phase. Suppressing olivenite from the calculations, a small geminite field appears at low pH and high Cu and As concentrations (Fig. 5b), as expected. These predictions agree with the occurrence and assemblages of geminite as a relatively abundant secondary mineral in Jáchymov (Škácha *et al.*, 2019; Majzlan *et al.*, 2020).

Limited natural observations on aqueous solutions that precipitate $M[AsO_3(OH)]{\cdot}H_2O$ minerals support our findings. Recently, we have described solutions that precipitate cobaltkoritnigite [(Co,Zn)[$AsO_3(OH)$]·H_2O] in underground spaces in Jáchymov, Czech Republic (Majzlan *et al.*, 2020, their tables 2 and 3). The pH of these two solutions were 2.41 and 2.96. Calculations with *PHREEQC* (Parkhurst and Appelo, 1999; LLNL database) returned saturation indices for koritnigite of –0.48 and +0.78. This result proves that a koritnigite-like phase is near equilibrium with these aqueous solutions, in good agreement with the active precipitation of cobaltkoritnigite at this site.

Haidingerite [$Ca[AsO_3(OH)]{\cdot}H_2O$] and the chemically related pharmacolite [$Ca[AsO_3(OH)]{\cdot}2H_2O$] are predicted to crystallise from Ca- and As-rich solutions (Majzlan *et al.*, 2020). In this case, however, their solubility is higher than for the $M[AsO_3(OH)]{\cdot}H_2O$ with M^{2+} = Cu, Zn or Mn. Because of the much larger ionic radius of Ca^{2+} (in comparison to Cu^{2+}, Zn^{2+} or Mn^{2+}), there are limited structural relationships between the systems CaO–As_2O_5–H_2O and those with CuO, ZnO, or MnO.

In the system MgO–As_2O_5–H_2O, the mineral magnesiokoritnigite [$Mg[AsO_3(OH)]{\cdot}H_2O$] was described recently by Kampf *et al.* (2013). It occurs together with anhydrite, halite, lavendulan, quartz and scorodite at the Torrecillas mine in the Atacama Desert in Chile. The association with scorodite and lavendulan suggests precipitation from acidic solutions and the presence of anhydrite implies low activity of H_2O, elevated formation temperature, low relative air humidity, or combination of such factors. The Atacama Desert is dry but not particularly hot (McKay *et al.*, 2003), with average temperatures of 16–17°C and air humidity of 25%. The humidity of the air and soil could occasionally increase during the rare rain events. Having recently derived a thermodynamic data set for brassite [$Mg[AsO_3(OH)]{\cdot}4H_2O$] and rösslerite [$Mg[AsO_3(OH)]{\cdot}7H_2O$] (Majzlan *et al.*, 2020), we can estimate roughly the thermodynamic properties of magnesiokoritnigite. Considering the reaction:

$$Mg[AsO_3(OH)]\cdot 4H_2O\ (cr) \rightarrow Mg[AsO_3(OH)]\cdot H_2O\ (cr) + 3H_2O\ (g).$$

If these phases are in equilibrium at 25°C and relative air humidity (RH) of 25%, the calculation gives $\Delta_f G°$(magnesiokoritnigite) of

https://doi.org/10.1180/mgm.2022.140 Published online by Cambridge University Press

−1418 kJ·mol^{-1} and the solubility product of −2.0. The equilibrium may lie at even lower air humidities and in that case, the solubility product would be higher. For example, if RH = 10%, then log K_{sp} = −0.9. We adopt log K_{sp} of −2.0 as a rough estimate and compare this value to the log K_{sp} values for other minerals in this group.

Field observations of assemblages with koritnigite and krautite

Our field observations in underground spaces in Jáchymov showed that precipitation of cobaltkoritnigite and koritnigite is connected to strongly acidic solutions (Majzlan *et al.*, 2020). They are derived from oxidative weathering of nickelskutterudite or krutovite in the absence of carbonate gangue minerals which could serve as a pH buffer. Cobaltkoritnigite seems much scarcer than koritnigite, in agreement with the general prevalence of Ni over Co in the ores in Jáchymov. As there are no carbonates as potential sources of Ca or Mn, haidingerite (which otherwise can precipitate under similar pH conditions as koritnigite) has never been observed together with koritnigite and its occurrences are linked to other locations in the mines.

Koritnigite and cobaltkoritnigite are rarely associated with the vivianite-group minerals köttigite and erythrite. The latter minerals should form from mildly acidic or neutral solutions and grow centimetres to decimetres away from the koritnigite and cobaltkoritnigite aggregates. Such associations document strong pH gradients over short distances that could be driven only by neutralisation by primary carbonates in specific local environments.

Krautite occurs in the same parts of the galleries of the Geschieber vein in the Svornost mine as koritnigite and cobaltkoritnigite. The source of Mn is probably a small amount of the gangue carbonates. This notion could be supported by the fact that unlike cobaltkoritnigite/koritnigite, which occur without any directly associated secondary phases, krautite usually grows on gypsum crystals. Therefore, both Ca and Mn can be derived from the dissolved carbonates. Calcium reacts preferably with sulfate in the solution to form gypsum, whereas Mn, and probably also Zn and Co, prefer the arsenates structures of the krautite-type.

Acknowledgements. We appreciate the comments of two anonymous reviewers who helped to improve the manuscript. This work was supported financially by a *Deutsche Forschungsgemeinschaft* grant MA 3927/42-1. The support to J.P. through the Operational Programme of the MEYS CR (Project No. SOLID21 CZ.02. 1.01/0.0/0.0/16_019/0000760) is acknowledged.

Supplementary material. To view supplementary material for this article, please visit https://doi.org/10.1180/mgm.2022.140

Competing interests. The authors declare none.

References

Bergerhoff G., Berndt M., Brandenburg K. and Degen T. (1999) Concerning inorganic crystal structure types. *Acta Crystallographica,* **B55**, 147–156.

Bramwell S.T., Buckley A.M., Visser D. and Day P. (1988) Magnetic susceptibility study of $KNiAsO_4$, $HMnAsO_4{\cdot}H_2O$ and their organic-intercalated derivatives. *Physics and Chemistry of Minerals*, **15**, 465–469.

Bramwell S.T., Buckley A.M., Rosseinsky M.J. and Day P. (1994) Neutron powder diffraction study of the crystal structure of the layered mineral krautite, $DMnAsO_4{\cdot}D_2O$. *New Journal of Chemistry*, **18**, 1209–1214.

Brown I.D. (2002) *The Chemical Bond in Inorganic Chemistry: The Bond Valence Model*. Oxford University Press, UK.

Brown I.D. (2009) Recent developments in the methods and applications of the bond valence model. *Chemical Reviews*, **109**, 6858–6919.

Buckley A.M., Bramwell S.T. and Day P. (1990) Intercalation reactions of krautite, $HMnAsO_4{\cdot}H_2O$. *American Mineralogist*, **75**, 1140–1146.

Cámara F., Biagioni C., Ciriotti M., Bosi F., Kolitsch U., Paar W., Hålenius U., Lepore G.O., Blass G. and Bittarello E. (2023) Piccoliite, $NaCaMn^{3+}_2(AsO^4)_2O(OH)$, a new arsenate from the manganese deposits of Montaldo di Mondovì and Valletta, Piedmont (Italy). *Mineralogical Magazine*, **87**, https://doi.org/10.1180/mgm.2022.129

Catti M. and Franchini-Angela M. (1979) Krautite, $Mn(H_2O)(AsO_3OH)$: Crystal structure, hydrogen bonding, and relations with haidingerite and pharmacolite. *American Mineralogist*, **64**, 1248–1254.

Ciesielczuk J., Janeczek J. and Szełęg E. (2018) Erythrite-köttigite extended solid solution. *IMA conference volume of abstracts*, **2018**, 189.

Cooper M.A. and Hawthorne F.C. (1995) The crystal structure of geminite, $Cu(AsO_3OH)(H_2O)$, a heteropolyhedral sheet structure. *The Canadian Mineralogist*, **33**, 1111–1118.

Dachs E. and Benisek A. (2011) A sample-saving method for heat capacity measurements on powders using relaxation calorimetry. *Cryogenics*, **51**, 460–464.

Deiss E. (1914) Ueber Herstellung und Eigenschaften der Manganoarsenatgallerte. *Kolloid-Zeitschrift*, **14**, 139–146.

Drahota P. and Filippi M. (2009) Secondary arsenic minerals in the environment: a review. *Environment International*, **35**, 1243–1255.

Dumańska-Słowik M., Pieczka A., Natkaniec-Nowak L., Kunecki P., Gaweł A., Heflik W., Smoliński W. and Kozub-Budzyń G. (2018) Mg-enriched erythrite from Bou Azzer, Anti-Atlas Mountains, Morocco: geochemical and spectroscopic characteristics. *Mineralogy and Petrology*, **112**, 381–392.

Fleck M., Kolitsch U. and Hertweck B. (2002) Natural and synthetic compounds with kröhnkite-type chains: Review and classification. *Zeitschrift für Kristallographie*, **217**, 435–443.

Fontan F., Orliac M. and Permingeat F. (1975) La krautite $MnHAsO_4{\cdot}H_2O$, une nouvelle espèce minérale. *Bulletin de la Société Française de Minéralogie et de Cristallographie*, **98**, 78–84.

Gagné O.C. and Hawthorne F.C. (2015) Comprehensive derivation of bond-valence parameters for ion pairs involving oxygen. *Acta Crystallographica*, **B71**, 562–578.

Gatuingt L., Rossano S., Mertz J.-D., Fourdrin C., Rozenbaum O., Lemasson Q., Reguer S., Trcera N. and Lanson B. (2021) Characterization and origin of the Mn-rich patinas formed on Lunéville château sandstones. *European Journal of Mineralogy*, **33**, 687–702.

Hawthorne F.C. (1992) The role of OH and H_2O in oxide and oxysalt minerals. *Zeitschrift für Kristallographie*, **201**, 183–206.

Hawthorne F.C. (2012) A bond-topological approach to theoretical mineralogy: crystal structure, chemical composition and chemical reactions. *Physics and Chemistry of Minerals*, **39**, 841–874.

Hawthorne F.C. and Schindler M. (2008) Understanding the weakly bonded constituents in oxysalt minerals. *Zeitschrift für Kristallographie*, **223**, 41–68.

Hawthorne F.C. and Sokolova E. (2012) The role of H_2O in controlling bond topology: I. The $^{[6]}Mg(SO_4)(H_2O)_n$ (n = 0–11) structures. *Zeitschrift für Kristallographie*, **227**, 594–603.

Holtstam D., Bindi L., Förster H., Karlsson A. and Gatedal K. (2022) Garpenbergite, $Mn_6\square As_5Sb_5O_{10}(OH)_2$, a new mineral related to manganostibite, from the Garpenberg Zn–Pb–Ag deposit, Sweden. *Mineralogical Magazine*, **86**, 1–8.

Johnston R.B. and Singer P.C. (2007) Solubility of symplesite (ferrous arsenate): implications for reduced groundwaters and other geochemical environments. *Soil Science Society of American Journal*, **71**, 101–107.

Kampf A.R., Nash B.P., Dini M. and Donoso A.A.M. (2013) Magnesiokoritnigite, $Mg(AsO_3OH){\cdot}H_2O$, from the Torrecillas mine, Iquique Province, Chile: the Mg-analogue of koritnigite. *Mineralogical Magazine*, **77**, 3081–3092.

Keller P., Hess H. and Riffel H. (1980) Die Kristallstruktur von Koritnigit, $Zn[H_2O|HOAsO_3]$. *Neues Jahrbuch für Mineralogie, Abhandlungen*, **138**, 316–332.

Kennedy C.A., Stancescu M., Marriott R.A. and White M.A. (2007) Recommendations for accurate heat capacity measurements using a Quantum Design physical property measurement system. *Cryogenics*, **47**, 107–112.

Lee J.S. and Nriagu J.O. (2007) Stability constants for metal arsenates. *Environmental Chemistry*, **4**, 123–133.

Lide D.R. (editor) (2005) *Handbook of Chemistry and Physics*. 85th ed. CRC Press, Boca Raton, USA.

Magalhães M.C.F., De Jesus J.D.P. and Williams P.A. (1988) The chemistry of formation of some secondary arsenate minerals of Cu(II), Zn(II) and Pb(II). *Mineralogical Magazine*, **52**, 679–690.

Majzlan J. (2017) Solution calorimetry on minerals related to acid mine drainage – methodology, checks, and balances. *Acta Geologica Slovaca*, **9**, 171–183.

Majzlan J., Fillipi M. and Drahota P. (2014) Mineralogy and crystal chemistry of arsenic. Pp. 17–184 in: *Arsenic: Environmental Geochemistry, Mineralogy, and Microbiology* (Robert J. Bowell, Charles N. Alpers, Heather E. Jamieson, D. Kirk Nordstrom and Juraj Majzlan, editors). Reviews in Mineralogy and Geochemistry, **79**. Mineralogical Society of America and the Geochemical Society, Chantilly, Virginia, USA.

Majzlan J., Plášil J., Dachs E., Benisek A., Mangold S., Škoda R. and Abrosimova N. (2020) Prediction and observation of formation of Ca-Mg arsenates in acidic and alkaline fluids: Thermodynamic properties and mineral assemblages in Jáchymov, Czech Republic and Rotgülden, Austria. *Chemical Geology*, **559**, 119922.

McKay C.P., Friedmann E.I., Gómez-Silva B., Cáceres-Villanueva L., Andersen D.T. and Landheim R. (2003) Temperature and moisture conditions for life in the extreme arid region of the Atacama Desert: Four years of observations including the El Niño of 1997–1998. *Astrobiology*, **3**, 393–405.

Nordstrom D.K., Königsberger E. and Majzlan J. (2014) Thermodynamic Properties for Arsenic Minerals and Aqueous Species. Pp. 217–255 in: *Arsenic: Environmental Geochemistry, Mineralogy, and Microbiology* (Robert J. Bowell, Charles N. Alpers, Heather E. Jamieson, D. Kirk Nordstrom and Juraj Majzlan, editors). Reviews in Mineralogy and Geochemistry, **79**. Mineralogical Society of America and the Geochemical Society, Chantilly, Virginia, USA.

Parkhurst D.L. and Appelo C.A.J. (1999) User's guide to PHREEQC (Version 2): A computer program for speciation, batch-reaction, one-dimensional transport, and inverse geochemical calculations. *Water-Research Investigation Report*, **99**, 312 p.

Petříček V., Dušek M. and Palatinus L. (2014) Crystallographic computing system JANA2006: general features. *Zeitschrift für Kristallographie*, **229**, 345–352.

Petříček V., Dus˘ek M. and Plás˘il J. (2016) Crystallographic computing system Jana2006: solution and refinement of twinned structures. *Zeitschrift für Kristallographie*, **231**, 583–599.

Petříček V., Dušek M. and Palatinus L. (2020) *Crystallographic computing system JANA2020*. Institute of Physics of the CAS, Prague, Czech Republic.

Plášil J., Škácha P., Sejkora J., Škoda R., Novák M., Veselovský F. and Hloušek J. (2017) Babánekite, $Cu_3(AsO_4)_2{\cdot}8H_2O$, from Jáchymov, Czech Republic - a new member of the vivianite group. *Journal of Geosciences*, **62**, 261–270.

Plumhoff A., Dachs E., Benisek A., Plášil J., Sejkora J., Števko M. and Majzlan J. (2020) Thermodynamic properties, crystal structure and phase relations of pushcharovskite $[Cu(AsO_3OH)(H_2O){\cdot}0.5H_2O]$, geminite $[Cu(AsO_3OH)(H_2O)]$ and liroconite $[Cu_2Al(AsO_4)(OH)_4{\cdot}4H_2O]$. *European Journal of Mineralogy*, **32**, 285–304.

Robie R.A. and Hemingway B.S. (1995) Thermodynamic properties of minerals and related substances at 298.15 K and 1 bar (105 Pascals) and at higher temperatures. *U.S. Geological Survey Bulletin*, **2131**, 461 pp.

Schindler M. and Hawthorne F.C. (2008) The stereochemistry and chemical composition of interstitial complexes in uranyl-oxysalt minerals. *The Canadian Mineralogist*, **46**, 467–501.

Sejkora J., Bureš B. and Hykš J. (2014) An occurrence of Mn-rich köttigite at the area of Marie and Geyer veins, Svornost, Jáchymov (Czech Republic). *Bulletin Mineralogie a Petrologie*, **22**, 233–239.

Shapiro J.L., Woodfield B.F., Stevens R. and Boerio-Goates J. (1999) Molar heat capacity and thermodynamic functions of the type II antiferromagnet MnO. *Journal of Chemical Thermodynamics*, **31**, 725–739.

Sheldrick G.M. (2015) SHELXT – integrated space-group and crystal-structure determination. *Acta Crystallographica*, **A71**, 3–8.

Siuda R. and Macioch A. (2018): Secondary arsenic minerals from the Złoty Stok As-Au abandoned mine (SW Poland). *Geological Quarterly*, **62**, 925–940.

Škácha P., Plášil J. and Horák V. (2019) *Jáchymov – a mineralogical pearl of Krušné Hory Mts*. Academia, Madrid, Spain, 682 pp.

Southwood M., Števko M. and Carr P. (2020) Tsumeb: Zincolivenite and the adamite-olivenite series. *Rocks & Minerals*, **95**, 210–232.

Tournassat C., Charlet L., Bosbach D. and Manceau A. (2002) Arsenic(III) oxidation by birnessite and precipitation of manganese(II) arsenate. *Environmental Science & Technology*, **36**, 493–500.

Weil M., Kolitsch U. and Stürzer T. (2022) Dimorphism of $MnHAsO_4(H_2O)$: natural monoclinic krautite and its synthetic triclinic modification. *Zeitschrift für Naturforschung*, **77**, 221–230.

Zettler F., Riffel H., Hess H. and Keller P. (1979) Cobalt(II) hydrogen arsenate monohydrate. Preparation and crystal structure. *Zeitschrift für Anorganische und Allgemeine Chemie*, **454**, 134–144.

https://doi.org/10.1180/mgm.2022.140 Published online by Cambridge University Press